

Thermodynamic study and transition metal (nickel) doping on $\text{Li}_{1.2}\text{Mn}_{0.8}\text{O}_2$ as a cathode material

Vusani Mikosi^{1}, Kemeridge Malatji¹, Noko Ngoepe¹, and Phuti Ngoepe¹*

¹Materials Modelling Centre, University of Limpopo, Private Bag x1106, Sovenga, 0727, South Africa

Abstract. Several studies have been conducted to overcome the poor cycling stability, voltage fade, and low coulombic efficiency barriers in practical applications of Lithium manganese oxides. Transition metal doping is considered as one of the effective techniques to enhance the stability of these materials. In this study we use the genetic algorithm within cluster expansion to generate new phases of Ni-doped $\text{Li}_{1.2}\text{Mn}_{0.8}\text{O}_2$ which was constructed from Li_2MnO_3 . Li_2MnO_3 's high energy density and high specific capacity have drawn attention to the material as a promising cathode for lithium-ion batteries. The generated phases are thermodynamically stable with negative heats of formation. Furthermore, first principles calculations were performed to study the thermodynamic, mechanical, and electronic properties of these materials. The materials were found to be thermodynamically stable with negative heats of formation and mechanically stable under the strain 0.001. Furthermore, the generated phases show an improvement on the conductivity of the $\text{Li}_{1.2}\text{Mn}_{0.8}\text{O}_2$ since they do not have band gaps suggesting that they are conductors.

1 Introduction

Lithium-ion batteries (LIBs) have become highly dependable as energy storage sources for transport grid applications due to their high energy density and high energy capacity ranging from 200-250W h/kg [1]. With the rising development of electric vehicles and smart grids, there is an increasing demand in the development of high performing LIBs [2].

[*mikosivusi@gmail.com](mailto:mikosivusi@gmail.com)

Since the cathode material is one of the primary components that determine the performance of LIBs and the cathode material contributes largely to the composition of the battery and thus influence the energy density [3], it is essential to develop cathode materials with higher specific capacity to improve the energy density of the batteries. Li-rich Mn-based layered oxide cathodes (LLO) have attracted wide attention as promising cathodes for LIBs due to their ability to deliver high theoretical specific capacity $>300\text{mAhg}^{-1}$, reversible specific capacity $>250\text{mAhg}^{-1}$ and energy density of $>1000\text{Wh/kg}$ as well as their environmental safety and low cost [4] [5].

However, these LLOs experience some unwanted disturbances associated with the redox process, which happen naturally when the upper cut-off voltage is in the range 4.6-4.8V [6]. They suffer from capacity fading, voltage decay, and low coulombic efficiency which results from the layered to spinel structural transformation and cation rearrangements caused by activation of Li_2MnO_3 and consequently irreversible Li-ion removal and oxygen loss [7] [8]. Several techniques such as elemental doping, surface modification, and coating have been employed in a quest to address these issues [9]. However, finding acceptable cathode materials with stable structural compositions and good properties is still a challenge, and as such materials such as LiCoO_2 , LiNiO_2 , and LiMnO_2 are being studied and a satisfactory outcome is yet to be found [10].

In this study we investigate the structural, thermodynamic, mechanical, and electronic properties of the layered $\text{Li}_{1.2}\text{Mn}_{0.8}\text{O}_2$ structure which was constructed from the layered Li_2MnO_3 . We further investigate the effects of the presence of Ni in improving the stability of $\text{Li}_{1.2}\text{Mn}_{0.8}\text{O}_2$ by doping the structure with Ni on the manganese site and thereafter performing the thermodynamic, mechanical, and electronic property calculations of the structures containing Nickel.

2 Methodology

This study was done computationally based on the density functional theory (DFT) framework [11]. To calculate the structural, thermodynamic, mechanical, and electronic properties of all the structures, we used the Vienna ab initio simulation package (VASP) code [12]. The correlation function that was used with these calculations is the Generalized Gradient Approximation (GGA) parametrized by Perdew-Burke Ernzerhof (PBE) [13] [14]. Geometry optimization of the structure $\text{Li}_{1.2}\text{Mn}_{0.8}\text{O}_2$ was done with the plane wave basis set of 10^{-7}eV and cut off energy of 500eV along with the Brillouin zone sampling scheme of Monk horst-pack with $4\times 4\times 4$ k-mesh parameters.

The structures with Ni were optimized with 500eV cut-off energy and k-mesh parameters of $2\times 2\times 2$. The Hubbard parameter within the Local Density Approximation (LDA+U) was applied with $U=5\text{eV}$ and $J=1\text{eV}$ for the metal Mn with respect to the structure $\text{Li}_{1.2}\text{Mn}_{0.8}\text{O}_2$ was applied to accurately reproduce the Mn-3d states. The cluster expansions were performed within the Universal Cluster Expansion (UNCLE) [15] code which allows set up, construction, and convergence of a cluster expansion for bulk or surface systems. This code was used to generate new structures of Ni-doped $\text{Li}_{1.2}\text{Mn}_{0.8}\text{O}_2$ structure and to predict the most stable phase.

3 Results and discussions

3.1 Structural analysis

The crystal structure was optimized before any calculations were performed, allowing the atom positions to relax, the cell volume to change, and allowing the cell shape to change. This full geometry relaxation of the atoms was done to obtain the lattice parameters and energy of formation at the ground state level. Figure 1 below is a representation of the optimized $\text{Li}_{1.2}\text{Mn}_{0.8}\text{O}_2$ structure. Table 1 shows the obtained values of the lattice parameters, the energy of formation, and the cell volume. The material is a monoclinic crystal belonging to the space group P2. This is solidified by the lattice parameters which are in the form $a \neq b \neq c$ and $\alpha = \gamma = 90^\circ \neq \beta$. A negative energy of formation corresponds to thermal stability of a material, therefore, the more negative the energy of formation is for a material, the greater its thermal stability. The negative value of energy of formation of the structure $\text{Li}_{1.2}\text{Mn}_{0.8}\text{O}_2$ indicates that it is thermally stable.

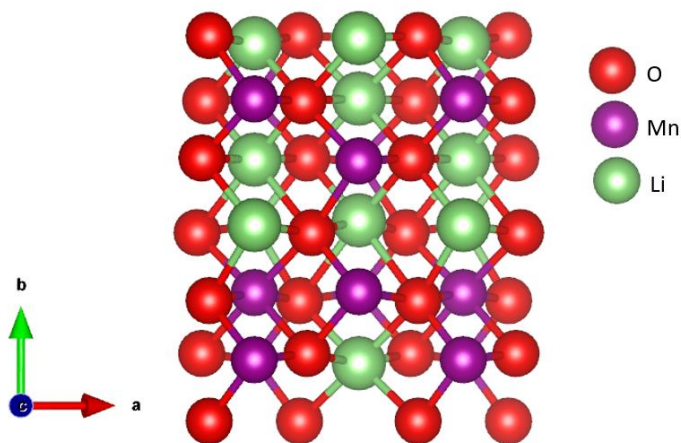


Fig. 1. Optimized structure of $\text{Li}_{1.2}\text{Mn}_{0.8}\text{O}_2$.

Table 1: Calculated lattice parameters, cell volume, and energy of formation of the $\text{Li}_{1.2}\text{Mn}_{0.8}\text{O}_2$ structure.

Parameter	Value
a	5.066
b	8.874
c	5.059
α	90.000°
β	108.179
γ	90.000°
Energy of formation (kJ/mol)	-4090.78
Volume (Å^3)	216.107

3.2 Mechanical stability

The elastic constants were calculated to investigate the mechanical stability of the material. These elastic constants were calculated under a strain of 0.001. For the material to be considered mechanically stable with reference to the elastic constants, it must satisfy the mechanical stability criteria for its crystal shape. For monoclinic crystals the stability criteria is given by:

$$(C_{44}C_{66} - C_{46}^2) > 0 \quad (1)$$

$$(C_{35}C_{55} - C_{35}^2) > 0 \quad (2)$$

$$(C_{22} + C_{33} - 2C_{23}) > 0 \quad (3)$$

$$[C_{11} + C_{22} + C_{33} + 2(C_{12} + C_{13} + C_{23})] > 0 \quad (4)$$

$$[C_{22}(C_{33}C_{55} - C_{35}^2) + 2C_{23}C_{25}C_{35} - C_{23}^2C_{55} - C_{25}^2C_{33}] > 0 \quad (5)$$

The constants also need to satisfy $C_{11}>0$, $C_{22}>0$, $C_{33}>0$, $C_{44}>0$, $C_{55}>0$, $C_{66}>0$ [16].

Incorporating the obtained elastic constants displayed in table 2 below into the above equations, all conditions are satisfied. This suggests that the material is mechanically stable. To further evaluate the mechanical stability, the elastic moduli was considered. Table 3 shows the obtained values for bulk, shear, and Young's modulus for this material. These values suggest that $\text{Li}_{1.2}\text{Mn}_{0.8}\text{O}_2$ has high compressive strength, is stiff, and it is resistant to elastic deformation. Although the elastic constants and the elastic moduli suggest that the material is mechanically stable, the Pugh ratio predicts the material to be brittle implying that it will be subjected to failure before deformation occurs when it undergoes large amounts of plastic deformation. The material is brittle since the obtained Pugh's ratio is less than

1.75 and for a material to be considered ductile its Pugh’s ratio must be >1.75, otherwise it is brittle [17].

Table 2: Elastic constants of $\text{Li}_{1.2}\text{Mn}_{0.8}\text{O}_2$ structure.

Elastic constants	$\text{Li}_{1.2}\text{Mn}_{0.8}\text{O}_2$
C_{11}	277.58
C_{12}	81.87
C_{13}	85.11
C_{15}	6.26
C_{22}	246.05
C_{23}	89.46
C_{25}	30.23
C_{33}	257.89
C_{35}	18.49
C_{44}	78.51
C_{46}	11.27
C_{55}	96.45
C_{66}	84.7

Table 3: Elastic moduli and Pugh's ratio of $\text{Li}_{1.2}\text{Mn}_{0.8}\text{O}_2$ structure.

	Bulk (GPa)	Shear (GPa)	Young's (GPa)	B/G
$\text{Li}_{1.2}\text{Mn}_{0.8}\text{O}_2$	143.82	86.96	217.11	1.65

3.3 Density of states

The density of states of a material is essential in studying the electronic behaviour of the material. It is possible to deduce the whether the material is an electric insulator, semiconductor, or a conductor by evaluating the density of states of the electrons since the electronic structure of a material determines its electrical conduction properties [18]. The electronic stability of a material is attributed to the fermi level position, to the TDOS, and to the presence of a pseudopotential or band gap near the fermi level in the TDOS [19].

The total and partial density of states (TDOS, PDOS) of $\text{Li}_{1.2}\text{Mn}_{0.8}\text{O}_2$ is shown in figure 2 below. In this plot, the straight line at zero energy represents the fermi level. The PDOS of the Li atom shows that the Li atom has minimum contribution to the TDOS of the bulk structure. The d-orbital of the Li atom is the most dominant. The Mn-d orbital is the most dominant for the Mn atom. The d-orbital is dominant at fermi level and at the region between 1 to 2eV and -4 to -2eV. The Mn-d orbital has a higher density of states at these regions compared to the s-orbital, p-orbital and all the orbitals of the other atoms. This suggests that the Mn-d orbital has greater contribution to the density of states of the bulk material in the specified regions. The p-orbital dominates in the PDOS of the O atom. The increased intensity of peaks for the Mn-d orbital from 1eV to 1.5eV and O-p orbital from -3eV to -1.5eV is an

indication of strong interaction between the p and d orbitals of the O and Mn respectively [10]. According to the density of states, the material has an energy band gap of 0.269eV around the fermi level and this is evident in the TDOS plot in figure 2 below. The presence of this band gap indicates that the material is a semiconductor.

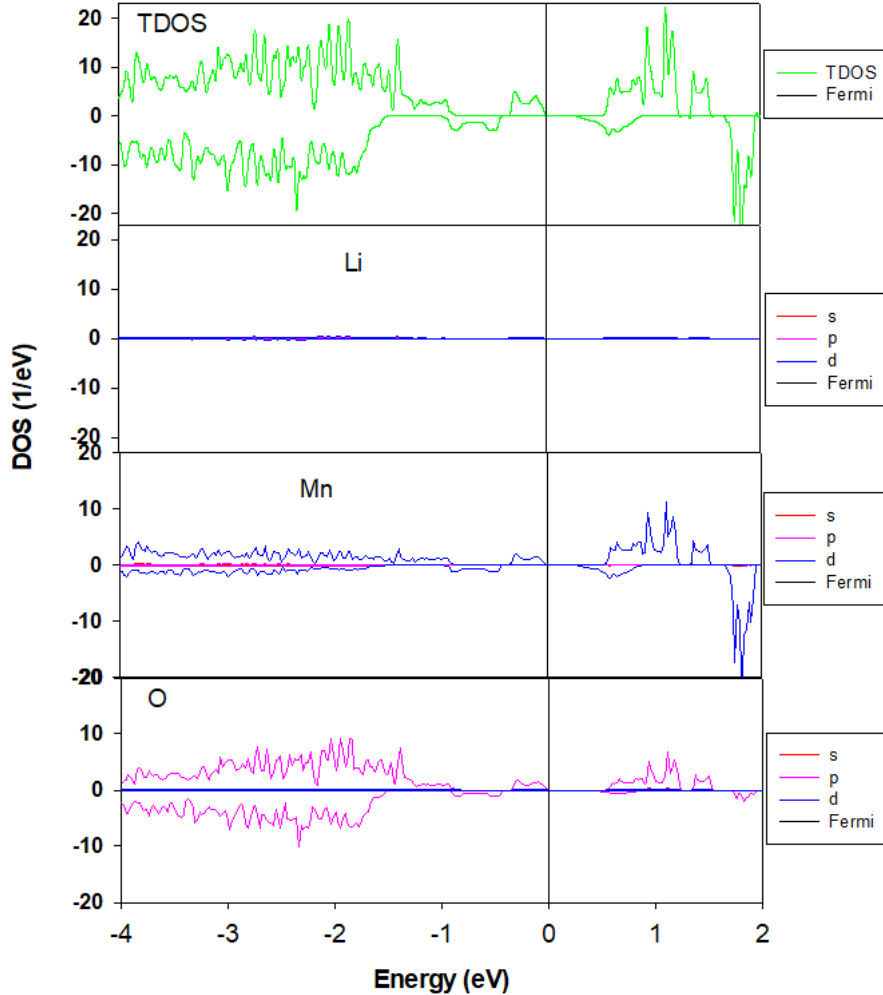


Fig. 2. The total and partial density of states of $\text{Li}_{1.2}\text{Mn}_{0.8}\text{O}_2$ structure.

3.4 Cluster expansion

We evaluated the effects of Ni doping on the structure $\text{Li}_{1.2}\text{Mn}_{0.8}\text{O}_2$. The structure was doped with Ni on all Mn sites yielding $\text{Li}_{1.2}\text{Mn}_{0.8}\text{Ni}_{0.8}\text{O}_2$. This structure was then subjected to cluster expansion which uses the genetic algorithm approach to generate new stable phases as shown in figure 3. The red line on the diagram represents the

binary ground state line. The grey crosses and the green crosses represent values predicted by the cluster expansion and values predicted for the training set structures respectively. The ground state search generated 12 new phases with negative heats of formation indicating thermodynamically stable and ordered structures. The binary ground state diagram shows that of the 12 generated phases, 2 phases $\text{Li}_{1.2}\text{Ni}_{0.5}\text{Mn}_{0.3}\text{O}_2$ and $\text{Li}_{1.2}\text{Ni}_{0.2}\text{Mn}_{0.6}\text{O}_2$ lie on the binary ground state line, and they are the stable. The phase $\text{Li}_{1.2}\text{Ni}_{0.5}\text{Mn}_{0.3}\text{O}_2$ with lowest energy of formation is positioned at $x=0.4$ on the binary diagram and is considered as the most stable generated phase with 40% Mn and 60% Ni concentration.

The iterative optimization progress of this cluster expansion is summarized in table 4 below. The table shows the number of iterations in this process, the number of structures used in each iteration, the number of new structures generated in each iteration, and the cross-validation score (CVS). The CVS gives an indication of whether the cluster expansion was a good one or not. A good cluster expansion is indicated by CVS less than 5meV per position. As seen in column 4 of table 4, the CVS of the generated phases is 4.9meV/pos which is within the required 5meV/pos. This suggests that the phases were accurately predicted by cluster expansion.

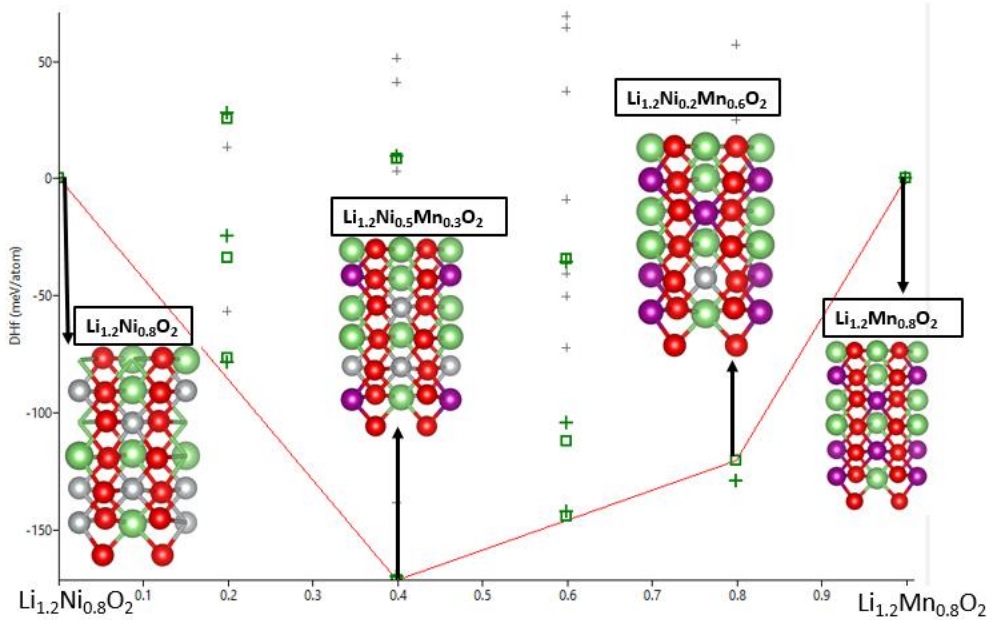


Fig. 3. The binary ground state diagram of the $\text{Li}_{1.2}\text{Mn}_{0.8}\text{Ni}_{0.8}\text{O}_2$ system.

Table 4: Summary of the iterative optimization progress for the genetic algorithm procedure.

Iteration	Number of structures	of	Number of new structures	CVS (meV/pos.)
0	0		2	-
0	0		11	-
1	11		1	4
2	12		0	4.9

4. Structural, mechanical, and electronic properties of the generated phases $\text{Li}_{1.2}\text{Ni}_{0.2}\text{Mn}_{0.6}\text{O}_2$ and $\text{Li}_{1.2}\text{Ni}_{0.5}\text{Mn}_{0.3}\text{O}_2$.

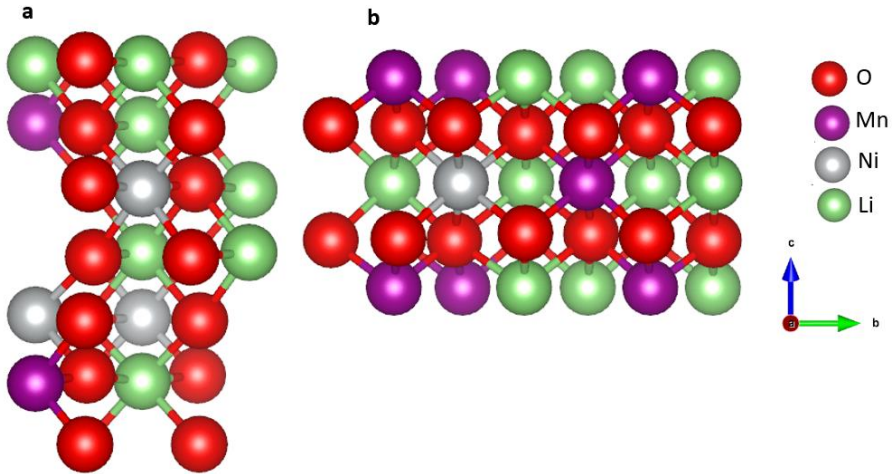


Fig. 4. Optimized crystal structures of (a) $\text{Li}_{1.2}\text{Ni}_{0.5}\text{Mn}_{0.3}\text{O}_2$ and (b) $\text{Li}_{1.2}\text{Ni}_{0.2}\text{Mn}_{0.6}\text{O}_2$.

4.1 Structural properties

Table 5 shows the structural properties of the 2 stable phases on the red DFT ground state line shown in figure 3. These stable structures $\text{Li}_{1.2}\text{Ni}_{0.2}\text{Mn}_{0.6}\text{O}_2$ and $\text{Li}_{1.2}\text{Ni}_{0.5}\text{Mn}_{0.3}\text{O}_2$ depicted in figure 4 are triclinic crystals with space group symmetries P2 and P1 respectively. $\text{Li}_{1.2}\text{Ni}_{0.5}\text{Mn}_{0.3}\text{O}_2$ shows to have a high formation energy as compared to that of the parent structure $\text{Li}_{1.2}\text{Mn}_{0.8}\text{O}_2$, implying less thermal stability. As displayed in table 5 below it is shown in comparison that the $\text{Li}_{1.2}\text{Ni}_{0.2}\text{Mn}_{0.6}\text{O}_2$ structure has the lowest formation energy, which suggests that it is the most thermally stable structure. It further shows that its energy of formation is lower than that of the parent structure $\text{Li}_{1.2}\text{Mn}_{0.8}\text{O}_2$ showing an improvement in thermal stability.

Table 5: Calculated lattice parameters, cell volume, and energy of formation of the $\text{Li}_{1.2}\text{Ni}_{0.2}\text{Mn}_{0.6}\text{O}_2$ and $\text{Li}_{1.2}\text{Ni}_{0.5}\text{Mn}_{0.3}\text{O}_2$ structures.

Parameter	Value	
	$\text{Li}_{1.2}\text{Ni}_{0.2}\text{Mn}_{0.6}\text{O}_2$	$\text{Li}_{1.2}\text{Ni}_{0.5}\text{Mn}_{0.3}\text{O}_2$
a	5.079	4.929
b	5.059	4.916
c	8.592	8.391
α	90.132°	90.004°
β	90.024°	90.032°
γ	110.834°	108.269°
Volume (\AA^3)	206.336	193.093
Energy of formation (kJ/mol)	-4465.09	-3901.45

4.2 Mechanical properties

The generated materials have a triclinic shape unlike the parent structure which has a monoclinic shape. As such, these materials need to satisfy the mechanical stability criteria of triclinic crystals for them to be considered mechanically stable. The stability criteria of triclinic crystals is given by: [20]

$$C_{11} > 0, C_{22} > 0, C_{33} > 0, C_{44} > 0, C_{55} > 0, C_{66} > 0 \tag{6}$$

$$[C_{11} + C_{22} + C_{33} + 2 \times (C_{12} + C_{13} + C_{23})] > 0 \tag{7}$$

$$(C_{33} \times C_{55} - C_{35}^2) > 0, (C_{44} \times C_{66} - C_{46}^2) > 0 \tag{8}$$

$$(C_{22} + C_{33} - 2 \times C_{23}) > 0 \tag{9}$$

Table 6 below details the obtained elastic constants of the two materials $\text{Li}_{1.2}\text{Ni}_{0.5}\text{Mn}_{0.3}\text{O}_2$ and $\text{Li}_{1.2}\text{Ni}_{0.2}\text{Mn}_{0.6}\text{O}_2$. These elastic constants were calculated under a strain of 0.001. The obtained elastic constants for $\text{Li}_{1.2}\text{Ni}_{0.5}\text{Mn}_{0.3}\text{O}_2$ satisfy the all the mechanical stability conditions listed above. On the other hand, $\text{Li}_{1.2}\text{Ni}_{0.2}\text{Mn}_{0.6}\text{O}_2$ meets all the conditions except for $C_{44}>0$ since its C_{44} value is negative. These results suggest that for the strain 0.001 $\text{Li}_{1.2}\text{Ni}_{0.5}\text{Mn}_{0.3}\text{O}_2$ is mechanically stable and $\text{Li}_{1.2}\text{Ni}_{0.2}\text{Mn}_{0.6}\text{O}_2$ is mechanically unstable.

Table 6: Elastic constants of $\text{Li}_{1.2}\text{Ni}_{0.5}\text{Mn}_{0.3}\text{O}_2$ and $\text{Li}_{1.2}\text{Ni}_{0.2}\text{Mn}_{0.6}\text{O}_2$ structures.

Elastic Constant (C_{ij})	$\text{Li}_{1.2}\text{Ni}_{0.5}\text{Mn}_{0.3}\text{O}_2$	$\text{Li}_{1.2}\text{Ni}_{0.2}\text{Mn}_{0.6}\text{O}_2$
C_{11}	198.68	274.54
C_{12}	-31.23	68.23
C_{13}	153.70	57.54
C_{14}	0.36	0.00
C_{15}	121.51	4.04
C_{16}	-94.36	0.03
C_{22}	26.46	270.87
C_{23}	69.67	62.39
C_{24}	-29.89	0.01
C_{25}	141.36	11.08
C_{26}	-116.00	0.05
C_{33}	283.22	255.83
C_{34}	3.12	0.01
C_{35}	145.45	1.12
C_{36}	-7.10	0.05
C_{44}	64.66	-68.12
C_{45}	-2.55	-0.00
C_{46}	-4.72	-4.00
C_{55}	176.22	97.47
C_{56}	26.62	-0.01
C_{66}	79.05	102.05

The elastic moduli were calculated to further analyse the mechanical stability of these generated materials. The elastic moduli is displayed in table 7 below. The bulk, shear, and young's moduli values of $\text{Li}_{1.2}\text{Ni}_{0.5}\text{Mn}_{0.3}\text{O}_2$ are all less than those of the parent structure $\text{Li}_{1.2}\text{Mn}_{0.8}\text{O}_2$. This implies that with $\text{Li}_{1.2}\text{Ni}_{0.5}\text{Mn}_{0.3}\text{O}_2$ the compressive strength, stiffness, and resistance to elastic deformation is reduced. With $\text{Li}_{1.2}\text{Ni}_{0.2}\text{Mn}_{0.6}\text{O}_2$ the shear and young's moduli values are higher than those of the parent structure, it is only the bulk modulus value that decreased. this means that with

this material the stiffness and the resistance to elastic deformation is improved whereas the compressive strength is reduced. Furthermore, we looked at the Pugh's ratio which gives the physical property of a material in terms of the material being ductile or brittle. Both materials are brittle since their Pugh's ratios are less than 1.75.

Table 7: Elastic moduli and Pugh's ratio of $\text{Li}_{1.2}\text{Ni}_{0.5}\text{Mn}_{0.3}\text{O}_2$ and $\text{Li}_{1.2}\text{Ni}_{0.2}\text{Mn}_{0.6}\text{O}_2$ structures.

Structure	Bulk (GPa)	Shear (GPa)	Young's (GPa)	B/G
$\text{Li}_{1.2}\text{Ni}_{0.5}\text{Mn}_{0.3}\text{O}_2$	99.18	85.07	198.46	1.17
$\text{Li}_{1.2}\text{Ni}_{0.2}\text{Mn}_{0.6}\text{O}_2$	130.84	94.40	228.2	1.39

4.3 Electronic properties

The TDOS and PDOS of the structures $\text{Li}_{1.2}\text{Ni}_{0.5}\text{Mn}_{0.3}\text{O}_2$ and $\text{Li}_{1.2}\text{Ni}_{0.2}\text{Mn}_{0.6}\text{O}_2$ are shown in figure 5 below. In the DOS plot of $\text{Li}_{1.2}\text{Ni}_{0.5}\text{Mn}_{0.3}\text{O}_2$, the PDOS of the Mn-atom is dominated by the d-states, these 3-d states of Mn are partially occupied with 5 electrons. The Mn-s and Mn-p states show minimum contribution to the total DOS.

The d-states are dominant in the Ni PDOS, these d-states are more filled than those of the Mn atom which accounts for the more intense peaks in Ni than Mn. On the other hand, the s and p states have minimum contribution. The Ni-d states have high intensity peaks at the region -0.5eV to -1.5eV. These peaks resemble the peak of the TDOS at -0.5eV to -1.5eV, implying that the Ni d-states have greater contribution to the TDOS at -0.5eV to -1.5eV.

With the Mn-atom the intensified peaks are at the region between 0.5eV to 1.5eV and they also resemble the shape of the peaks in the TDOS at this region 0.5eV to 1.5eV suggesting that the contribution of the Mn-d states to the TDOS is at 0.5eV to 1.5eV.

The O-p states are the most dominant in the O PDOS. The O-p states have the most intense peaks between -4eV and -2eV as compared to the Ni, Mn, and Li. They also have the same shape as that of the TDOS at -4eV and -2eV meaning that the O p-states are the ones contributing to the TDOS -4eV and -2eV. The Li-atom is dominated by the d-states regardless of its minimum contribution. As seen in the TDOS, the Fermi cuts the peak at the top and there is no pseudo-gap at the Fermi level. The TDOS suggests that the material $\text{Li}_{1.2}\text{Ni}_{0.5}\text{Mn}_{0.3}\text{O}_2$ is a magnetic metal.

The total density of states of $\text{Li}_{1.2}\text{Ni}_{0.2}\text{Mn}_{0.6}\text{O}_2$ and the PDOS of the Ni and the Mn atoms show dominance of the d-states. The Mn d-states have high peaks in both the valence band and the conduction band between -2.5eV to -0.2eV and 0eV to 1eV. The Ni d-states have high peaks between -1.8eV to -1eV, however, the peaks are not higher than those of the Mn d-states implying that the Mn d-states have greater contribution.

The O atom is dominated by the p-states, and these have intensified peaks at -4eV to -2.5eV with a shape like that of the TDOS at -4eV to -2.5eV. The Li atom has minimum contribution just as in $\text{Li}_{1.2}\text{Ni}_{0.5}\text{Mn}_{0.3}\text{O}_2$. The Fermi level cuts the peak at the top as seen in figure 5. This material does not have a band gap at the Fermi level. The structure is a half-metallic ferromagnet. As a result, it can act as a conductor with the electrons of one spin orientation and as an insulator or semiconductor with the

electrons of the other spin. In this material, bands for spin 1 are metallic and bands for spin 2 are semiconducting.

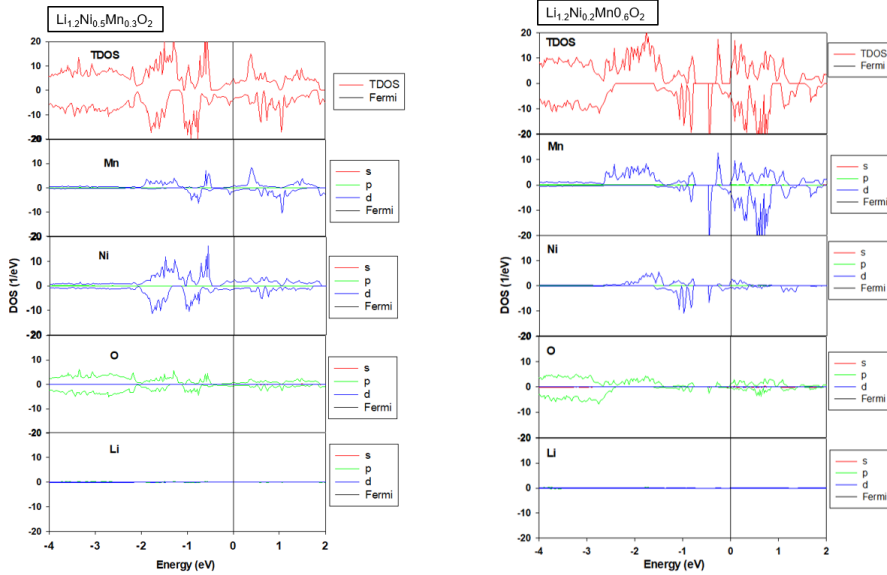


Fig. 5. Total and partial density of states of the $\text{Li}_{1.2}\text{Ni}_{0.5}\text{Mn}_{0.3}\text{O}_2$ and $\text{Li}_{1.2}\text{Ni}_{0.2}\text{Mn}_{0.6}\text{O}_2$ structures.

5. Conclusion

The genetic algorithm approach was successfully able to generate stable phases of the Ni-doped $\text{Li}_{1.2}\text{Mn}_{0.8}\text{O}_2$ structure. Structural, mechanical, and electronic properties of the parent structure $\text{Li}_{1.2}\text{Mn}_{0.8}\text{O}_2$ and the generated $\text{Li}_{1.2}\text{Ni}_{0.5}\text{Mn}_{0.3}\text{O}_2$ and $\text{Li}_{1.2}\text{Ni}_{0.2}\text{Mn}_{0.6}\text{O}_2$ were systematically calculated using first Principles calculation. $\text{Li}_{1.2}\text{Mn}_{0.8}\text{O}_2$ was found to be thermally stable with a negative energy of formation (-4090.78kJ/mol). The generated materials also had negative energies indicating thermal stability, however $\text{Li}_{1.2}\text{Ni}_{0.5}\text{Mn}_{0.3}\text{O}_2$ has a less negative value (-3901.45 kJ/mol) than $\text{Li}_{1.2}\text{Mn}_{0.8}\text{O}_2$ structure implying that with $\text{Li}_{1.2}\text{Ni}_{0.5}\text{Mn}_{0.3}\text{O}_2$ the thermal stability is reduced. $\text{Li}_{1.2}\text{Ni}_{0.2}\text{Mn}_{0.6}\text{O}_2$ on the other has a more negative value (-4465.09kJ/mol) than the parent structure indicating an improvement in the thermal stability. The mechanical properties calculations showed that the generated structures $\text{Li}_{1.2}\text{Ni}_{0.5}\text{Mn}_{0.3}\text{O}_2$ and $\text{Li}_{1.2}\text{Ni}_{0.2}\text{Mn}_{0.6}\text{O}_2$ are less mechanically stable than the initial structure $\text{Li}_{1.2}\text{Mn}_{0.8}\text{O}_2$ under the elastic strain 0.001. furthermore, the Pugh ratio showed that the generated materials are more brittle compared to the parent structure. The density of states shows that there is an improvement in conductivity with the generated materials that have no band gaps at the Fermi level unlike the parent structure which has a band gap of 0.269eV making it a semiconductor. Overall, doping the structure $\text{Li}_{1.2}\text{Mn}_{0.8}\text{O}_2$ with Ni reduces the Mn-O bond length which results in the observed improved stability.

Future work

As a result of the findings, the future work will be to dope the generated materials with a metal in a quest to decrease the brittleness of the materials and make them ductile. Furthermore, to add a metal that will improve the elastic stability of the generated materials.

Acknowledgements

The Materials Modelling Centre at University of Limpopo and the Centre for High Performance Computing (CHPC) are appreciated for their facilities which were used to carry out this work. The National Research Foundation is appreciated for financial support.

References

1. M. Shahjalal, P.K. Roy, T. Shams, A. Fly, J.I. Chowdhury, M.d.R. Ahmed, K. Liu, *Energy*. **241**, 122881 (2022)
2. L. Nie, S. Chen, W. Liu, *Nano Res.* **16**, 391-402 (2023)
3. W. Fu, D. Kim, F. Wang, G. Yushin, *J. Power Sources*. **561**, 232738 (2023)
4. H. Zheng, X. Han, W. Guo, L. Lin, Q. Xie, P. Liu, W. He, L. Wang, D.L. Peng, *Mater. Today Energy*. **18**, 100518 (2020)
5. Y. Wang, W. Yu, L. Zhao, A. Wu, A. Li, X. Dong, H. Huang, *Electrochim. Acta*. **461**, 142664 (2023)
6. A.R. Armstrong, M. Holzapfel, P. Novák, C.S. Johnson, S.H. Kang, M.M. Thackeray, and P.G. Bruce, *J. Am. Chem. Soc.* **128**, 8694-8698 (2006)
7. A. Boulineau, L. Simonin, J.F. Colin, E. Canévet, L. Daniel, S. Patoux, *Chem. Mater.* **24**, 3558-3566 (2012)
8. D. Mohanty, J. Li, D.P. Abraham, A. Huq, E. A. Payzant, D.L. Wood III, C. Daniel, *Chem. Mater.* **26**, 6272-6280 (2014)
9. H. Zheng, X. Han, W. Guo, L. Lin, Q. Xie, P. Liu, W. He, L. Wang, D.L. Peng, *Mater. Today Energy*. **18**, 100518 (2020)
10. C.I. Azambou, F.H.K. Djioko, O.O. Obiukwu, P.K. Tsobnang, E.E. Kalu, I.T. Kenfack, E.E.I Oguzie, *Mater. Today Commun.* **35**, 105738 (2023)
11. S. Kurth, M.A.L. Marques, E.K.U. Gross, *Encycl. Condens. Matter. Phys.* **9**, 395-405 (2005)
12. W. Yi, G. Tang, X. Chen, B. Yang, X. Liu, *Comp. Phys. Commun.* **257**, 107-124 (2020)
13. A.D. Becke, *Phys. Rev. A*. **38**, 3098-3100 (1988)

14. J.P. Perdew, K. Burke, M. Ernzerhof, *Phys. Rev. Lett.* **77**, 3865 (1996)
15. D. Lerch, O. Wiecekhorst, G.L.W. Hart, R.W. Forcade, S. Müller, *Model. Simul Mat Sci Eng.* **17**, 055003 (2009)
16. H.J. Wu, E.J. Zhao, H.P. Xiang, X.F. Hao, X.J. Liu, J. Meng, *Phys. Rev. B.* **76**, 15 2(007)
17. Q. Mahmood, M. Hassan, M. Rashid, B.U. Haq, A. Laref, *Phys. B: Condens Matter.* **571**, 87-92 (2019)
18. R. Marchiori, *Nanostruct.* **15**, 209-232 (2017)
19. P. Mao, B. Yu, Z. Liu, F. Wang, Y. Ju, *J. Appl. Phys.* **117**, 115903 (2015)
20. G. Qing, L.K. Chun, P. Ravindra, *J. Phys. Chem. C.* **123**, 4674-4681 (2019)